Environmental and Experimental Botany 133 (2017) 12–23

Contents lists available at ScienceDirect

Environmental and Experimental Botany

journal homepage: www.elsevier.com/locate/envexpbot

Arbuscular mycorrhizal fungi alter Hg root uptake and ligand environment as studied by X-ray absorption fine structure

Alojz Kodre[a,b], Iztok Arčon[b,c], Marta Debeljak[d], Mateja Potisek[e], Matevž Likar[e], Katarina Vogel-Mikuš[b,e,*]

[a] University of Ljubljana, Faculty of Mathematics & Physics, Jadranska 19, Ljubljana, Slovenia
[b] Jozef Stefan Institute, Jamova 39, Ljubljana, Slovenia
[c] University of Nova Gorica, Vipavska 13, Nova Gorica, Slovenia
[d] National Institute of Chemistry, Hajdrihova 19, Ljubljana, Slovenia
[e] University of Ljubljana, Biotechnical Faculty, Jamnikarjeva 101, Ljubljana, Slovenia

ARTICLE INFO

Article history:
Received 17 July 2016
Received in revised form 19 September 2016
Accepted 20 September 2016
Available online 21 September 2016

Keywords:
EXAFS
XANES
Arbuscular mycorrhiza
Phytoremediation
Toxicity
Hg coordination
Ligand environment

ABSTRACT

Mercury (Hg) – plant – fungal interactions are only poorly studied. Hg speciation and ligand environment in maize roots inoculated with arbuscular mycorrhizal (AM) fungi were investigated in order to better understand the role of AM in Hg soil to root transfer.

The maize plants were grown in Hg polluted substrate (50 $\mu g\, g^{-1}$ as dissolved $HgCl_2$) and inoculated with AM fungi originating from: a) highly Hg polluted environment of a former Hg smelting site in Idrija, Slovenia, (*Glomus* sp. – sample AmI), and b) non-polluted environment (commercial AM inoculum Symbivit® – sample AmC). Hg speciation and ligand environment in maize roots was studied by Hg-L_3 XANES and EXAFS with emphasis on XAS methodology – modelling and fitting the XAFS spectra to extract in a reliable way as much information on Hg coordination as possible.

The AmI plants developed more arbuscules and less vesicles than the AmC plants, and also accumulated more Hg in the roots. A clear difference in Hg coordination between the AM (AmC & AmI) and the control (ConC & ConI) plants is recognized in Hg L_3-edge EXAFS analysis: in the ConC & ConI maize roots 73–80% of Hg is attached between two sulphur atoms at the distance of 2.34 Å. The remaining ligand is nitrogen at 2.04 Å. In AmI & AmC roots another Hg-S attachment encompassing four thiol groups at the S-distance of ~2.50 Å are identified, accounting for 21–26%. AM fungi can modify Hg ligand environment in plant roots, thus playing an important role in biogeochemical cycling of Hg in terrestrial ecosystems.

1. Introduction

Mercury (Hg) is one of the most toxic and hazardous metals found in environment. For its mobility and persistence it is considered a global pollutant. It accumulates in food webs with biomagnification pattern posing a threat to human and animal health (Adriano, 2001). The occurrence of Hg polluted soils is associated either with natural deposition or anthropogenic dispersion from mining and smelting activities as in the case of Idrija in Slovenia or Almaden in Spain (Carrasco-Gil et al., 2013; Miklavčič et al., 2013; Morel et al., 1998).

Hg can be found in environment as a metal (Hg^0), in ionic form (Hg^{2+}), or as a constituent in metal ores (*e.g.* cinnabar, HgS). Its methylated forms (CH_3Hg^+, $(CH_3)_2Hg$), exert the highest toxic effect in animals and humans (Clarkson, 1972). Hg transformations, generally through reduction or methylation and demethylation, strongly depend on environmental conditions and affect its toxicity and distribution in the environment (Clarkson, 1972).

Phytostabilization is an *in situ* technology involving soil amendment and metal-tolerant plants to establish a ground cover that can reduce migration of metals to air, surface and ground

Abbreviations: AM, arbuscular mycorrhiza; EXAFS, extended X-ray absorption fine structure; XANES, X-ray absorption near edge structure; AmI, maize plants inoculated with AM fungi from Hg polluted Idrija site; AmC, maize plants inoculated with commercial AM fungal mixture; ConI, maize plants inoculated with soil bacteria extracted from Hg polluted Idrija site; ConC, maize plants inoculated with soil bacteria extracted from commercial AM inoculum; Con, maize plants grown in sterile soil.

* Corresponding author at: University of Ljubljana, Biotechnical Faculty, Jamnikarjeva 101, Ljubljana, Slovenia.
E-mail address: katarina.vogelmikus@bf.uni-lj.si (K. Vogel-Mikuš).

http://dx.doi.org/10.1016/j.envexpbot.2016.09.006
0098-8472/

water and reduce soil toxicity. The roots of plants with excluder metal tolerance strategy provide binding sites for metals that are either sequestred in the vacuoles of root cortical cells or bound to the cell wall components (Barceló and Poschenrieder, 2003). It has been shown that a properly developed mutual symbiosis between suitable fungal endophytes and plants (mycorrhiza) improving nutrient and water acquisition and providing protection from metal toxicity (Audet and Charest, 2007; Rajkumar et al., 2012) may be crucial for the survival of plants in metal polluted areas. Among fungal endophytes, mycorrhizal fungi form the most intimate relationship with plants. Owing to their metal tolerance they have been found in great abundance in the roots of the plants from metal-enriched sites. In addition to mycorrhiza, dark septate endophytes may also assist in conferring tolerance to the plants in metal polluted environments (Likar and Regvar, 2013). Mycorrhizal fungi play an important role in biogeochemical cycling of metals in terrestrial ecosystems (Rhee et al., 2012). Introducing suitable plant-fungal systems to Hg- contaminated sites may therefore help to retain Hg in the soil or in the root system and lower Hg transfer from the soil to the above-ground plant parts as well as from the soil directly to the atmosphere via volatilization.

Knowledge about distribution and speciation of toxic metals in plants is of fundamental importance for understanding the accumulation and transport mechanisms and in turn for optimization of plant performance in phytostabilization technologies. The existing synchrotron radiation facilities offer optimal possibilities to get insight into metal distribution and speciation in plants via synchrotron X-ray fluorescence microscopy and X-ray absorption spectroscopy (XAS) (Gräfe et al., 2014; Koren et al., 2013; Vogel-Mikuš et al., 2010). The latter provides a suitable tool, sensitized to a particular target atom by the choice of the energy range of the absorption scan in the vicinity of the target absorption edge. With fluorescence detection mode the method can be extended to trace concentrations of heavy metal pollutants. The absorption signal, in adjacent spectral regions of XANES and EXAFS, carries the fingerprints of the immediate chemical surroundings of the target atom, with its ligands directly recognizable. In XANES method, the measured profile of the absorption edge is compared to the corresponding segments in the absorption spectra of standards – candidate chemical compounds of the metal.

The EXAFS signal is an interference pattern impressed onto a typically ~1000 eV track of the absorption spectrum above the edge. The signal is compared to a synthetic spectrum built from a hypothetic arrangement of the neighbour atoms to the target metal atom.

Hg-L_3 edge EXAFS and XANES have already been proven useful tools for determination of Hg speciation and ligand environment in different plants grown under natural and controlled conditions (Carrasco-Gil et al., 2013; Patty et al., 2009; Rajan et al., 2008). Under natural conditions Hg accumulates mainly in the roots (Carrasco-Gil et al., 2013; Debeljak et al., 2013). In *Marrubium vulgare* collected at the Hg polluted area in Almaden, Spain, Hg was found localized in outer root layers, namely rhizodermis, mainly in the form of HgS minerals, which were also the prevailing Hg species found in the surrounding soils (Carrasco-Gil et al., 2013). HgS formation was supposedly facilitated by sulphate reducing bacteria, or was attributed to the root surface contamination by soil particles (Carrasco-Gil et al., 2013). In hydroponics, however, Hg was accumulated in roots mainly in the form of thiol compounds (C-S-Hg-S-C coordination) (Carrasco-Gil et al., 2013) and mainly localized in the cell walls. It is probably bound to the structural proteins such as expansins and extensins, which contain characteristic cystein-rich regions and play an important role in maintaining cell wall structure, integrity and normal functioning (Carrasco-Gil et al., 2013). Binding of Hg to these proteins is also in line with the observed root deformation caused by Hg. In a XANES study of Hg methylation in shredded *Eichornia crassipes*, the technique of linear combination fit (LCF) of XANES spectra with spectra of methylated and (in)organic Hg(II) model compounds revealed that in plants grown in aerobic conditions $5 \pm 3\%$ of Hg was in methylated form, while in the shredded plants in anaerobic conditions the percentage of methyl-Hg increased to $22 \pm 6\%$. The rest of Hg was bound to thiol (-SH) ligands (Rajan et al., 2008). In hydroponically grown *Spartina* cordgrass Hg was mainly bound as Hg(II)-cysteine, as methyl-mercury acetate and, interestingly, as HgS (cinnabar and meta-cinnabar) (Patty et al., 2009). The authors claim that HgS formation by sulphate reducing bacteria in the plant rhizosphere is well established and has a potential for phytostabilization of Hg, since Hg complexation into the highly insoluble HgS would reduce leaching as well as Hg volatilization (Patty et al., 2009). Although plants as well as fungi possess enzymatic machinery for sulphate reduction, and sulphide ion (S^{2-}) or H_2S is one of the intermediates in transformation of inorganic sulphur compounds, there is only little direct evidence on actual HgS formation in plants or fungi.

In the present study, using Hg L_3-edge EXAFS and XANES, the speciation and ligand environment of the metal in plants inoculated with a mixture of AM fungal strains (*Glomus* sp.) originating from highly Hg polluted environment of a former Hg smelting site in Idrija, Slovenia, and non-polluted environment (commercial AM inoculum Symbivit®) is correlated to the Hg uptake and the level of mycorrhization. In the aim to estimate the effects of mycorrhization on Hg soil-plant mobility, we hypothesized from the literature data (Audet and Charest, 2007) that AM fungi may at the soil Hg concentrations of 50 mg kg^{-1} help to retain Hg in the soil by extramatrical mycelium, possibly as HgS complex (Carrasco-Gil et al., 2013), and suppress the transfer to the roots. The experiment showed a rather different picture. With this in mind we spent additional efforts on XAS methodology – modelling and fitting the spectra to extract in a reliable way as much information on Hg coordination as possible. The problem in application of the XAS method to the present study is the wide choice of candidate ligand atoms to Hg: C, N, O, S, P – to remain just within normal biochemistry. It means that there is no fixed, well-defined set of standards for XANES, and that a large number of candidate atomic neighbourhood need to be tested in EXAFS analysis. Moreover, in a sample from a living plant, a number of different ligands should be expected, their fingerprints separable only *a posteriori* in the analysis of the measured signal.

The task is somewhat simplified in the combination of the two methods. XANES method can be efficiently used to sort out the ligands not present in the sample. The method is not molecule-sensitive, just ligand-sensitive. It means, for example, that any monodentate Hg salt of a carboxylic acid and any complex to a –OH rich organic molecule will show the O- ligand fingerprint, with the rest of the molecule contributing only minor variations. It also means that presence of a molecular species in a sample cannot be proved with XANES alone, in spite of such claims in the literature (Arai et al., 2004; Patty et al., 2009; Rajan et al., 2008).

After weeding out with XANES, model Hg neighbourhoods for EXAFS analysis are constructed with the remaining collection of ligands, with preference to molecules known as Hg immobilisers. In the present case, sulphur is the best candidate, followed by nitrogen and oxygen. The ligand carbon, in methyl-Hg derivates, is well documented for its toxicity (Clarkson, 1972), but is supposed to be below the detection level (<5%) in the present case, with the plants grown in well aerated substrate. The testing of model neighbourhoods in the EXAFS analysis has been largely inspired by the excellent study of Hg-DNA interaction by B. Ravel et al. (Ravel et al., 2009).

2. Materials & methods

2.1. Pot experiment

Maize was chosen as a model plant species for this pot experiment because of simple cultivation and high mycorrhizal potential of the plant. Maize seeds (variety DKC4014, provided by a local farmer) were surface sterilized in 10% sodium hypochlorite (NaOCl) for 10 min, rinsed with sterile distilled water, and sown in tall pots (ϕ 7 cm, height 20 cm) filled with premixed plant-growth substrate. The basis was a commercial substrate with 7.45 g kg^{-1} N, 2.64 g kg^{-1} P_2O_5, 2.67 g kg^{-1} K_2O, pH 6.9–7.2 and 252 g kg^{-1} organic matter (Biobrazda; Slovenia), preliminarily sterilized by autoclaving for 60 min at 121 °C, twice within a period of 48 h.

One half of the substrate was contaminated with 50 mg kg^{-1} of Hg (as $HgCl_2$ dissolved in water) and incubated for four weeks in a plastic bag, while the other half was retained non-contaminated (the control). Each half was further divided into five parts, to be inoculated in sequence with: 1) 5 g of AM fungal mixture from Hg-polluted site in the region of Idrija mercury mine in Slovenia [sample AmI]; 2) 5 g of commercial AM fungal mixture [sample AmC]; 3) soil bacterial extract from the Hg-polluted Idrija site [sample ConI]; 4) soil bacterial extract from commercial AM fungal mixture [sample ConC]; 5) non-inoculated, sterile soil [sample Con]. The plants were grown in pots for three months in a greenhouse under day light, supplemented by a red/blue LED diode light (16/8 day night photoperiod, 200 μmol m^{-2} s^{-1}), T = 15–23 °C (night/day), relative humidity 60%). For each treatment five pots were sown with 7-10 seeds and 7 days after germination 5 plants per pot were retained till the end of experiment.

2.2. Arbuscular mycorrhizal fungi inoculum preparation

Arbuscular mycorrhizal (AM) fungi were isolated from Hg polluted site in the region of Idrija mercury mine in Slovenia. The inoculum was prepared by "trap culture" system. AM fungi were isolated from the rhizospehere soil and roots of *Centaurea jacea* L. collected near the chimney of the cinnabar smelter in Idrija (field soil properties: sandy loam, total Hg as measured by XRF (Nečemer et al., 2008); 120 ± 12 μg Hg g^{-1} dry weight, pH 7.5, organic matter 30 g kg^{-1}). The roots were cut to 1–2 cm fragments and mixed with rhizosphere soil and further mixed with commercial pot substrate (Biobrazda; Slovenia, described above) in the ratio 1:2. The commercial substrate was previously sterilized by autoclaving for 60 min at 121 °C, twice within a period of 48 h. Maize plants (*Zea mays* L.) were grown in this mixture for three months in order to enable multiplication of AM strains. Idrija inoculum (AmI) contained AM fungal strains belonging to *Glomus* sp. as determined PCR analysis (see below). Symbivit® was used as commercial AM inoculum (AmC) and contained a mixture of *G. intraradices* BEG140, *G. mosseae* BEG95, *G. etunicatum* BEG92, *G. claroideum* BEG96, *G. microaggregatum* BEG56, *G. geosporum* BEG199 (http://www.inoculumplus.eu/nos-produits-en/symbivit).

Bacterial inocula were prepared by mixing AM inocula (from Idrija or the commercial inoculum) with sterile water (1:10). The suspension was then filtered through the sieves with 0.5, 0.2 and 0.1 mm pore size and then further through the sieve with 45 μm pore size in order to remove AM fungal propagules (hyphae, spores), but not the soil bacteria.

2.3. Characterization of AM inoculum from Idrija

2.3.1. PCR amplification

DNA was extracted from three subsamples of maize roots (equal to 30 mg dry weight in total) using GenElute Plant Genomic DNA miniprep kits (Sigma), following the manufacturer instructions. The 18S rDNA segment was amplified by nested PCR, first using the MH2 and MH4 primers (Vandenkoornhuyse and Leyval, 1998), and then the universal eukaryotic primer NS31 (Simon et al., 1992) with a mix of AMF-specific primers AM1, AM2 and AM3 (Helgason et al., 1998; Santos-González et al., 2007; Simon et al., 1992). The PCR protocol with MH2 and MH4 was: 95 °C for 2 min, followed by 32 cycles at 94 °C for 1 min, 48 °C (−0.1 °C for each cycle) for 1 min, 72 °C for 2 min, and final extension at 72 °C for 8 min. One microliter of the fungal DNA template was used in a final volume of 25 μl PCR mix, using 2.5 μl 10 × PCR buffer, 1.5 μM MgCl2, 200 μM of each nucleotide, 400 nM of each primer, and 1.25 U Taq polymerase (all Fermentas). The second (nested) PCR was performed with the same reaction mixture, using the NS31-AMmix primer set, and following the protocol of (Calvente et al., 2004): 95 °C for 2 min, followed by 30 cycles at 95 °C for 1 min, 62 °C for 1 min, 72 °C for 1 min, and final extension at 72 °C for 10 min.

Table 1
GenBank accession numbers of sequences from maize roots colonized by the AM fungi multiplied from *Centaurea jaccea* L. roots and rhizosphere soil collected at former Hg smelting site in Idrija, nearest matches, phylum affiliations and E values.

Acc. No	Nearest match			Max ident (%)
	Acc No	Acc	E	
KX38938	JQ218183	*Glomus sp.*	0.0	99
KX38939	JN009583	Glomeromycota	0.0	99
KX38940	JN009583	Glomeromycota	0.0	99
KX38941	JN009234	Glomeromycota	0.0	99
KX38942	KF939919	Glomeromycota	0.0	97
KX38943	JQ218183	*Glomus sp.*	0.0	98

2.3.2. Sequencing and analysis

The amplified 18S rDNA regions were cloned prior to sequencing by ligation of the PCR products into the pGEM-T easy vector (Promega, USA). The ligation product was cloned into competent JM109 cells and cultured on LB agar containing X-Gal/isopropyl-beta-D-thiogalactopyranoside and 50 μl/ml ampicillin (Sigma). Plasmid extraction was carried out from white colonies, and cloning was verified by colony PCR with the T7 and SP6 primers. Cycle-sequencing reactions were performed with the T7 and SP6 primers using BigDye terminator Ready Reaction Cycle Sequencing kits on an ABI 3730xl DNA analyser (Applied Biosystems), as provided by the Macrogen Company (Korea).

The sequences were subjected to GenBank search, using the default option of gapped-BLAST (Altschul et al., 1997), and aligned with the closest matches and additional representatives of the groups from GenBank. Maximum-likelihood analysis was performed using MEGA7 (Kumar et al., 2016). The robustness of the internal branches was assayed by bootstrap analysis (1000 runs). The evolutionary history was inferred by using the Maximum Likelihood method based on the Kimura 2-parameter model (Kimura, 1980). Sequencing revealed presence of AM fungi on the maize roots (Table 1). All identified AM fungal sequences were clustered in a separate cluster, next to *Glomus* group A sequences (Fig. 1).

2.4. Analysis of mycorrhizal colonization and Hg concentrations

At the end of the experiment the level of mycorrhizal colonization was assessed on 30–50 1 cm long root segments per treatment. After washing and clearing with 10% KOH, the roots were stained in 0.05% trypan blue according to the modified method of (Phillips and Hayman, 1970) and examined under a Karl Zeiss (KF 10) light microscope for abundance of particular structures (*e.g.* arbuscules, vesicles). Mycorrhizal frequency (F%) (% of colonized root fragments), mycorrhizal intensity (M%) (% of

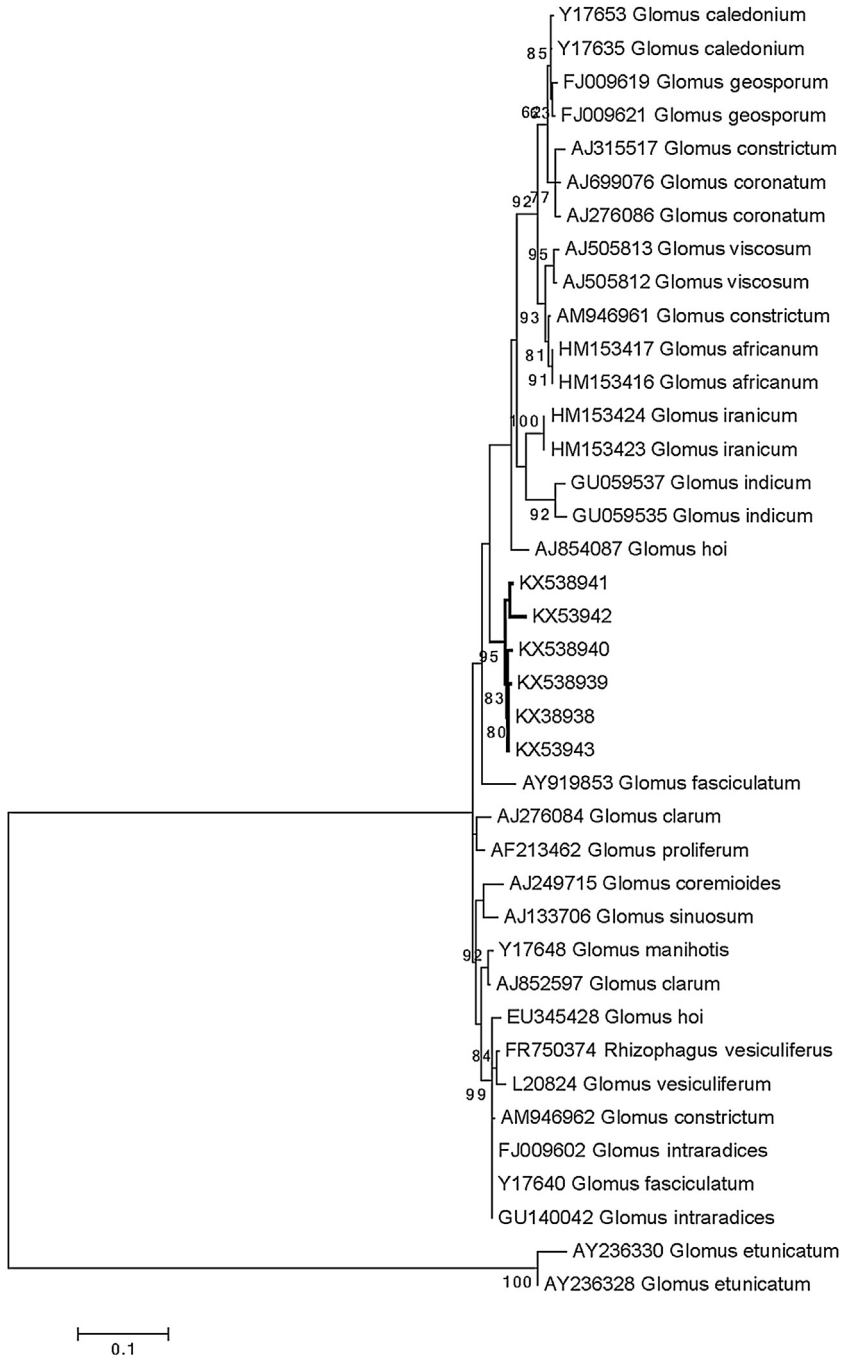

Fig. 1. Molecular Phylogenetic analysis of 18S rDNA amplified from maize roots colonized by the AM fungi multiplied from *Centaurea jaccea* roots and rhizosphere soil collected in Idrija by Maximum Likelihood method. The evolutionary history was inferred by using the Maximum Likelihood method based on the Kimura 2-parameter model. The tree with the highest log likelihood (−2407.9686) is shown. Initial tree(s) for the heuristic search were obtained automatically by applying Neighbour-Join and BioNJ algorithms to a matrix of pairwise distances estimated using the Maximum Composite Likelihood (MCL) approach, and then selecting the topology with superior log likelihood value. The tree is drawn to scale, with branch lengths measured in the number of substitutions per site. The analysis involved 39 nucleotide sequences. All positions containing gaps and missing data were eliminated. There were a total of 416 positions in the final dataset. Evolutionary analyses were conducted in MEGA7.

colonisation of particular root fragment), arbuscular density (A%) (% of arbuscules in particular root fragment expressed relatively to the rest of AM structures) and vesicular density (V%) (% of vesicles in particular root fragment expressed relatively to the rest of AM structures) were assessed according to Trouvelot et al. (1986). The level of colonisation by dark septate endophytic fungi (DSE%) was also assessed, in the same way as A% and V%.

Hg concentrations in roots were measured by ICP-MS (Inductively coupled plasma mass spectroscopy) after microwave assisted digestion in concentrated HNO_3 and stabilization of digests by HCl (Debeljak et al., 2013). The results were validated by measuring standard reference materials (BCR/CRM-061 Aquatic plant, NIST; ERM Tuna fish, Sigma Aldrich).

In order to provide a general model of Hg coordination in the fungal mycelium we attempted to collect AM extramatrical hyphae from the soil by wet sieving (Gaur and Varma, 2007), but at the end the amount was not enough to get sufficient signal for XANES/EXAFS analysis. Thus a strain of a dark septate fungal endophyte was grown for one month in axenic conditions in dark in liquid Melin-Norkrans-Marx medium supplemented with 100 μM Hg

(20,1 mg/kg) [sample Fung]. This strain was isolated from a willow (*Salix caprea*) and belongs to *Phialophora/Cadophora* and *Leptodontidium orchidicola complex* (Likar and Regvar, 2013).

2.5. XAS experiment

The above listed samples from fungal mycelia and from the roots of the maize plants were prepared for XAFS analysis by rapid freezing of the material in liquid nitrogen and subsequent freeze-drying in order to concentrate the samples for XAS measurements in fluorescence mode. The dried material was ground in a mortar with liquid nitrogen, pressed into self-standing pellets and stored in vacuum sealed bags at 4 °C till the measurements.

In addition, pellets of different Hg compounds were prepared, such as HgS and Hg-phosphate, and most notably, organic Hg complexes with histidine, cysteine, and cellulose as reference standards for N-, S-, and O-ligand environments. Cinnabar was obtained from mercury mine in Idrija: 20 mg of pulverized material was thoroughly mixed with 50 mg of microcrystalline cellulose. The standard complexes were prepared by mixing $HgCl_2$ by histidine, cysteine and cellulose in Hg: ligand molar ratio of 1:20. pH of mixtures was adjusted to 5.5.–6.0 in order to mimic the physiological pH. The solutions were then frozen and freeze-dried.

Hg L_3-edge EXAFS and XANES spectra of plant samples and standards (Hg-hystidine, Hg-cysteine, Hg-cellulose, Hg-pectine, Hg-phosphate) were measured at liquid nitrogen temperature in fluorescence detection mode at BM23 beamline of the ESRF synchrotron source in Grenoble, France, using He cryostat and thirteen-segment germanium solid state detector to collect fluorescence signal from the plant samples (Kodre et al., 2015; Vogel-Mikuš et al., 2010).

Reference Hg complexes were pressed into homogeneous pellets with total absorption thickness μd of about 2 above Hg L_3-edge (Koren et al., 2013). XAS spectra of HgS and $HgCl_2$ were measured in transmission detection mode at room temperature at XAFS beamline of Elettra synchrotron at Trieste, Italy. Double crystal Si(111) monochromator with energy resolution of about 1.5 eV at 12 keV was used at both sites. At BM23, higher harmonics in the beam were eliminated by a flat rhodium-coated mirror placed after the monochromator; at XAFS beamline of Elettra detuning of the second monochromator crystal was used. The intensity of the monochromatized beam was monitored with three ionization detectors: at BM23 beamline they were filled with argon (220 mbar, 754 mbar, and 1600 mbar), while at XAFS beamline of Elettra gas mixture was used (70 mbar Ar + 1000 mbar N2, 650 mbar Ar + 1350 mbar N_2, and 1620 mbar Ar + 380 mbar N2). In all detectors He was added to the total pressure of 2 bars. Samples were placed between the first pair of detectors, and the reference tungsten metal foil between the posterior pair, to check the stability of the energy scale and to obtain the exact energy calibration (W L_1 absorption edge: 12098 eV). The absolute energy reproducibility of the measured spectra was ±0.02 eV.

The absorption spectra were measured within the interval −250 eV–1,000 eV relative to the investigated absorption edge. In XANES region, equidistant energy steps of 0.3 eV were used, while for the EXAFS region, equidistant k-steps ($\Delta k \approx 0.03$ Å^{-1}) were adopted, with integration time of 1 s/step in transmission mode, and 4s/step in fluorescence detection mode. The spectra of two identical consecutive runs on a sample were superimposed to improve the signal-to-noise ratio and to check the stability and reproducibility of the detection system. The XANES and EXAFS spectra were analysed with the IFEFFIT package (Ravel and Newville, 2005).

2.6. Statistical analysis

Statistical analyses of data presented in Table 1 were performed by Statistica Statsoft 7.0 and XLSTAT software. Non-parametric Kruskal Wallis test was used for post hoc analysis. Cluster analysis based on Euclidian distances combined with heat map depicting relationships between AM parameters (A% – arbuscular density, V % – vesicular density), Hg concentrations and the percentage of di- and tetra-thiolate Hg complexes was generated in R i386 3.0.2 (using function heatmap.2, gplots package) after z-normalization of the data (Singh et al., 2014).

3. Results

3.1. Hg root uptake and mycorrhization of the plants

Plants inoculated with AM fungi (*Glomus* sp.) isolated from Hg contaminated soil collected at the nearest vicinity of former cinnabar smelter in Idrija, accumulated significantly more Hg than the plants inoculated with commercial inoculum (AmC) and the control plants (Con, ConC, ConI) (Table 1). This, however, was not reflected in the shoots, where very low Hg concentrations when compared to the roots were detected (0.8–1.4 μg g^{-1} dry mass). Despite relatively high substrate Hg concentrations used, root biomass was not significantly affected by Hg (data not shown), although there is a decrease of the root biomass in AmI plants (Table 2).

Arbuscular mycorrhizal structures (hyphae, arbuscules, vesicles) were present in roots of the plants inoculated with commercial AM fungal strains as well as AM fungal strains from Idrija. However, the level of formation of arbuscules (A%) that serve as an interface for nutrient exchange, was more pronounced in the plants inoculated with the AM fungal strains from Idrija (AmI) (Table 2). On the other hand the commercial fungal strains produced more vesicles, which served as storage and dormancy structures, indicating that these strains were not as well adapted to high Hg concentration in the soil as the strains isolated from Hg contaminated soil.

Isolated dark septate endophytes (DSE) fungus accumulated up to 3000 μg Hg g^{-1} (dry weight) when grown in a relatively highly Hg contaminated liquid medium (100 μM Hg as $HgCl_2$). Although

Table 2
Root biomass, Hg concentration, Hg content (mean ± se, n = 3–5) and % of arbuscular mycorrhizal colonisation (mycorrhizal frequency – F%, mycorrhizal intensity – M%, arbuscular density – A%, vesicular density – V%, DSE% – dark septate edophyte density; mean value, 30–50 root fragments examined per treatment) in Hg treated maize roots. Different letters besides the values indicate statistically significant differences (Kruskal-Wallis test, $p < 0.05$).

	Root biomass (g)	Root Hg (μg g^{-1})	Average root Hg content (μg plant^{-1})	F%	M%	A%	V%	DSE%
Con	1.03 ± 0.01	188 ± 9 a	185	0	0	0	0	
ConC	1.26 ± 0.17	183 ± 10 a	230	0	0	0	0	
ConI	1.24 ± 0.19	198 ± 17 a	245	0	0	0	0	
AmC	1.00 ± 0.10	220 ± 42 ab	220	100 ± 0	47 ± 3	16 ± 1a	27 ± 2b	10 ± 3
AmI	0.82 ± 0.07	439 ± 138 b	360	100 ± 0	39 ± 2	31 ± 2b	14 ± 1a	9 ± 3

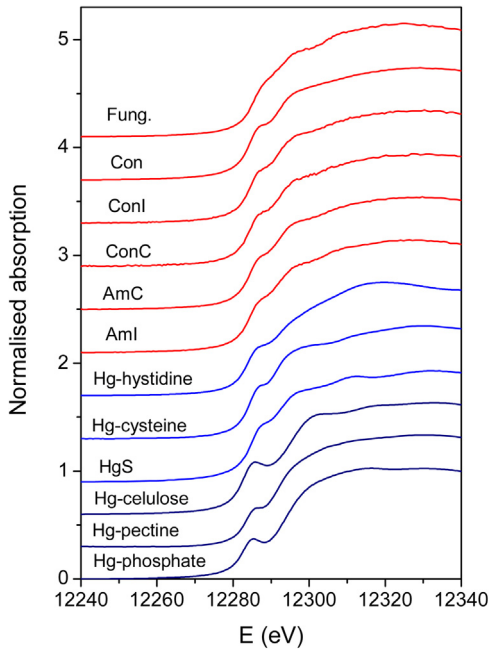

Fig. 2. XANES spectra of Hg reference compounds, plants (Con – plants grown in sterile soil, ConC- plants inoculated with bacteria from commercial AM inoculum, ConI – plants inoculated with bacteria from Idrija AM inoculum, AmC- plants inoculated with commercial AM inoculum, AmI – plants inoculated with Idrija AM inoculum) and fungi (Fung – dark septate endophyte grown in *in vitro* culture). The spectra are displaced vertically for clarity.

the growth of the fungus was suppressed in comparison to the control (data not shown), these results indicate that fungal mass can efficiently adsorb and/or absorb Hg from nutrient solution. Extrapolated to environmental conditions the results suggest that fungi with their fine hyphal network provide numerous binding sites for free Hg ions. The issue is further elucidated by XAFS study of Hg environment in mycorrhizal and non-mycorrhizal plants. The analysis is rather complex, proceeding in distinct steps.

3.2. XANES analysis

The analysis of XANES spectra was performed with the IFEFFIT program package ATHENA (Ravel and Newville, 2005). The relative L_3-shell contribution in the absorption spectra was obtained in the standard procedure (Ravel and Newville, 2005; Wong et al., 1984) by removing the extrapolated best-fit linear function determined in the pre-edge region (−150 eV to −30 eV), and by conventional normalization, extrapolating the post-edge spline background, determined in the range from 150 eV to 800 eV, to set the Hg L_3-edge jump to 1.

The spectra are plotted in Fig. 2 together with a selected set of XANES spectra of standard reference Hg complexes. The local environment of the Hg cation results in a distinct L_3-edge profile. Hg in plant tissues is expected to exhibit a combination of several profiles. To resolve the fingerprints of individual ligands *principal component analysis* (PCA) (Ravel and Newville, 2005) is used in the first step. The variation of the edge profile in the set of plant spectra is characterized by the correlations of pairs of spectra. In PCA eigenvectors of the correlation matrix of the target XANES spectra are extracted and ordered by the amount of total variance they account for. The number of the eigenvectors above the noise level denotes the true dimension of the vector space of the target spectra – i.e. the number of independent components with a physical meaning, possible Hg ligands in our case. Candidate components can be chosen from the spectra of those reference compounds and

Table 3
Eigenvalues obtained by principal component analysis (PCA) of the Hg L_3-edge XANES spectra of plant samples.

	Eigenvalues	Variance
1.	5.997267	0.999544
2.	0.002327	0.000388
3.	0.000164	0.000027
4.	0.000128	0.000021
5.	0.000083	0.000014
6.	0.000033	0.000005

complexes which lie entirely in the eigenvector space, i.e. do not introduce alien components.

The result of PCA is shown in Table 3. The inbuilt criterion in the Athena code decides for two principal components in our six target spectra. In our reference set, three candidates are found: Hg-cysteine, HgS and Hg-histidine. The first two represent a degenerate pair, both describing an S ligand, and the last one is an N-ligand. So, Hg-cysteine and Hg-histidine are chosen for the next step of analysis, the *linear combination fit* (LCF). The target spectra are projected onto the 2D subspace to determine the relative amount of either ligand. The quality of two-component fit of the XANES spectrum of ConI sample is illustrated in Fig. 3a. Same quality of fit is obtained also for other plants (Con, ConC, AmI, AmC). For fungal endophyte sample (Fung.), which exhibits recognisably different XANES profile, the two-component fit cannot completely reproduce all spectral features in the edge profile.

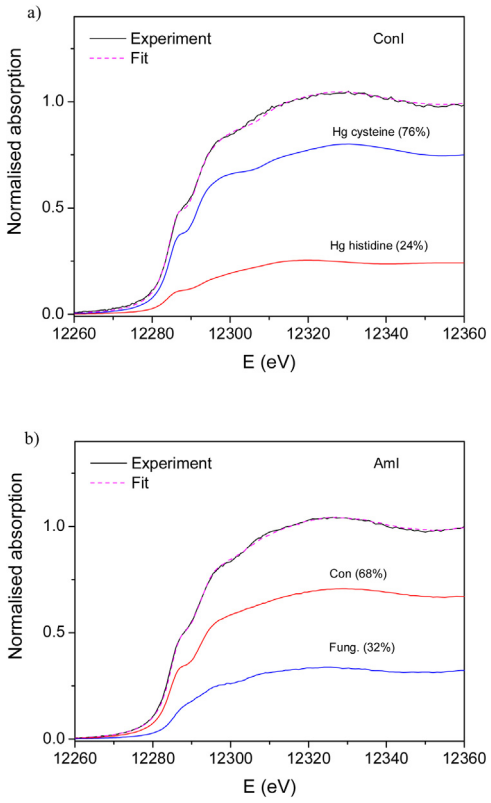

Fig. 3. a) The Hg L3-edge XANES spectrum measured on ConI sample. Black solid line – experiment; magenta dashed line – best-fit linear combination of XANES profiles of Hg-cysteine (74%) and Hg-histidine (24%). Fit components are shown below. b) The Hg L3-edge XANES spectrum measured on AmI sample. Black solid line – experiment; magenta dashed line – best-fit linear combination of XANES profiles of plant samples Con (68%) and fungal sample Fung (32%). Fit components are shown below.

Table 4
Relative amounts (%) of two Hg reference compounds that describe best linear combination fits for each Hg L_3-edge XANES spectra measured on plant tissues. Uncertainty is ±3%.

sample	Hg cysteine	Hg histidine
Con	81	19
ConC	71	29
ConI	76	24
AmC	72	28
AmI	67	33
Fung	53	47

Table 5
Relative amounts (%) of two plant/fungal spectra Con and Fung. that describe the rest of plant spectra by best linear combination fits. Uncertainty is ±2%.

sample	Con	Fung.
ConC	85	15
ConI	80	20
AmC	77	23
AmI	68	32

The fit results for all plant samples are listed in Table 4. The relative amounts of the two Hg reference compounds should not be interpreted as percentage of Hg bonding to cysteine or histidine: only as the percentages of S- and N-ligands at similar distances and similar neighbourhoods. The predicting power of PCA can be estimated in a simple test of including the third principal component, HgS into the LCF. The quality of the fit is generally improved, but the weight of S ligand is only redistributed between Hg-cysteine and HgS, leaving the N contribution mostly unchanged.

Interestingly, the two spectra Con and Fung, which show the largest difference in edge profiles in the plant/fungal series, can be used as references to describe the rest of plant spectra by a best linear combination fits, despite the fact that the Fung spectra was recorded on a DSE and not AM fungus. The quality of such a two-component fit of the XANES spectrum of AmI sample is illustrated in Fig. 3b. Same quality of fit is obtained also for the other plants spectra (ConC, ConI, AmC), Relative amounts (%) of the two components are listed in Table 5. The result gives an insight into the differences between individual XANES spectra in the plant series: i.e. to what extent are the inoculated plants spectra different from the spectrum of the plant grown on the non-inoculated, sterile soil [sample Con]. The difference can be described by a component expressed most strongly in fungal sample (Fung.). The samples AmC and AmI have 23% and 32% of Hg bound as in the fungal sample, respectively, correlating with the percentage of arbuscular density (A%) (Table 2). In the control samples ConI and ConC the percentage of Hg bound as in fungal sample was lower (Table 6).

3.3. EXAFS analysis

Additional insight in the Hg complexation in plant organs can be obtained by Hg L_3-EXAFS analysis, providing a quantitative description of the local structure around Hg atom.

Among the candidate elements for Hg close neighbours it is known that the affinity to S and N is stronger than that to O and C. Consequently, the binding to carboxylic acids can be assumed as of lesser importance, and, similarly, the binding to ubiquitous $-PO_4$. The methylation of Hg, leading to the particularly toxic and mobile form of the element, is a product of certain anaerobic bacteria, so it is assumed that in samples of well aerated plant parts Hg–C bond is present only in minor amount. We can, however, expect EXAFS signatures of more than one ligand in a sample: not that a single Hg atom is bound to N and S, but that the sample contains Hg atoms with either ligands.

The analysis is further complicated by the fact that the ligands with consecutive atomic numbers, such as O and N (and C, for that matter), or S and P, are not unambiguously resolved, especially in the relatively short k-space interval of a useful signal. The latter pair is not problematic, since there is no report of direct Hg–P bond,

Table 6
Best-fit model parameters of Hg-L_3 edge EXAFS spectra of the six plant/fungal samples and of Hg-cysteine for comparison. The model comprises a linear combinations of the three Hg model neighbourhood environments of the three Hg complexes: di-thiol ligands Hg-$(S_1\text{-}C_1)_2$, tetra-thiol ligands Hg-$(S_2\text{-}C_2)_4$, and two amino ligands Hg–$(N\text{-}C_N)_2$, varying their relative frequency (adding up to 1), the distance R of each neighbour from the central Hg atom, and the width of the radial distribution σ^2 of the neighbours. The effective zero energy of the photoelectron E_0 is added, together with the quality-of-fit factor (r-factor). The values in square brackets are not independently varied but restricted with a relation to other parameters. The amplitude reduction factor S_0^2 is fixed at the value of 0.93, determined on reference Hg-cysteine sample. The uncertainty of the last digit is given in parentheses.

	Con	ConC	ConI	AmC	AmI	Fung	cysteine
Di-thiolate Hg complex Hg$(\text{-}S_1\text{-}C_1)_2$							
rel. freq.	0.80(7)	0.73(7)	0.77(7)	0.63(7)	0.52(7)	0.13(7)	0.84(7)
R (S_1) [Å]	2.338(7)	2.338(7)	2.338(7)	2.338(7)	2.338(7)	2.338(7)	2.334(7)
σ^2 (S_1) [Å^2]	0.004(1)	0.004(1)	0.004(1)	0.004(1)	0.004(1)	0.004(1)	0.0008(3)
R (C_1) [Å]	3.90(2)	3.90(2)	3.86(2)	4.06(2)	4.056(2)	4.06(2)	3.93(1)
σ^2 (C_1) [Å^2]	0.008(2)	0.008(2)	0.008(2)	0.008(2)	0.008(2)	0.008(2)	0.03(2)
Tetra-thiolate Hg complex Hg$(\text{-}S_2\text{-}C_2)_4$							
rel. freq.				0.21(7)	0.26(7)	0.64(7)	
R (S_2) [Å]				2.50(1)	2.50(1)	2.50(1)	
σ^2 (S_2) [Å^2]				0.004(1)	0.004(1)	0.004(1)	
R (C_2) [Å]				4.33(2)	4.33(2)	4.33(2)	
σ^2 (C_2) [Å^2]				0.008(2)	0.008(2)	0.008(2)	
Di-amino Hg complex with Hg$(\text{-}N\text{-}C_N)_2$ or Hg complex with two N in heterocyclic amines							
rel. freq. (N)	0.20(7)	0.27(7)	0.23(7)	0. 16(9)	0.16(9)	0.24(9)	0.16(7)
R (N) [Å]	2.04(1)	2.04(1)	2.04(1)	2.04(1)	2.04(1)	2.04(1)	2.05(3)
σ^2 (N) [Å^2]	0.004(1)	0.004(1)	0.004(1)	0.004(1)	0.004(1)	0.004(1)	0.003(2)
rel. freq. (C_N)	0.34(7)	0.34(7)	0.34(7)	0.16(7)	0.01(1)	0.24(9)	0.16(7)
R (C_N) [Å]	3.01(9)	2.83(9)	2.78(3)	2.98(9)	2.98(9)	2.98(9)	3.06(9)
σ^2 (C_N) [Å^2]	0.008(2)	0.008(2)	0.008(2)	0.008(2)	0.008(2)	0.008(2)	0.005(4)
E0 [eV]	4.2(9)	2.0(9)	3.0(9)	4.2(9)	4.2(9)	3.4(9)	5.6(9)
r-factor	0.017	0.072	0.053	0.055	0.037	0.024	0.0091

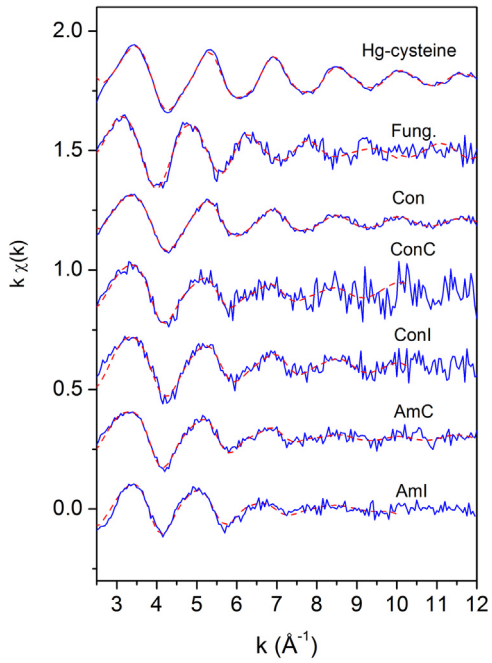

Fig. 4. The k^3 weighted Hg-L$_3$ edge EXAFS spectra measured on Hg-cysteine, plant (Con – plants grown in sterile soil, ConC- plants inoculated with bacteria from commercial AM inoculum, ConI – plants inoculated with bacteria from Idrija AM inoculum, AmC- plants inoculated with commercial AM inoculum, AmI – plants inoculated with Idrija AM inoculum) and fungal (Fung – dark septate endophyte grown in *in vitro* culture) samples. Solid line – experiment; dashed line – best fit EXAFS model. The spectra are displaced vertically for clarity.

but in the case N/O, there always remains the possibility of some carboxylic admixture hidden among the resolved nitrogen ligands.

Hg L$_3$-edge EXAFS spectra of the samples (Figs. 4 and 5) were analyzed with Artemis code (Ravel and Newville, 2005) of IFEFFIT. Initially, *ad hoc* FEFF models with the ligand element in the first shell and the radical C atom in the second shell were built. With the low concentration of Hg in the plant samples, the EXAFS signal was relatively weak, and even with prolonged detection time drowned in noise by k ~ 10 Å^{-1}. In combination with the R interval of 1.0–3.0 Å of the first peak in FT, the number of degrees of freedom in a fit was barely enough to determine the parameters of a single neighbour shell. To probe farther in the neighbourhood, some external information needed to be invoked whereby the additional parameters could be constrained or interrelated. The analysis of the reference samples (Hg-cellulose, Hg-histidine and Hg-cysteine), much less obscured by noise, provided good initial values of the ligand distances – 2.05 Å for O, 2.03 Å for N and 2.35 Å for S – and useful estimates for parameters of the second neighbours.

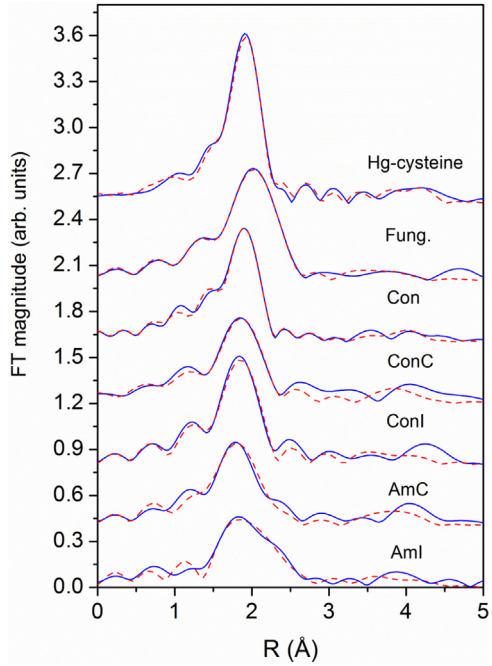

Fig. 5. Fourier transform magnitudes of the k^3 weighted Hg-L$_3$ edge EXAFS spectra from Fig. 2 (solid line), together with the best-fit EXAFS model (dashed line) calculated in the k range from 3 Å−1 to 12 Å−1 and R range from 1.0 Å to 4.4 Å. The spectra are displaced vertically for clarity. Sample tags are explained in the text.

We found thiol group –S–C as the dominant ligand in all plant samples, with S at ~2.35 Å and C atom at ~4 Å, in accord with the established –C–S distance of 1.82 Å and well in line with already published data (Manceau and Nagy, 2008; Nagy et al., 2011). The coordination number ~2 indicated two thiol groups to a Hg atom. The *ad hoc* model accounted for the larger part of the FT signal between 1 and 3 Å, with exception of the lowermost part of the fitting interval at 1 Å indicating some contribution of the nearer ligands N or O. In the fungal sample (Fung), the S neighbour was detected at a larger average distance 2.43 Å.

3.4. The Hg-cysteine S/N model

To establish a firm base for the analysis of the plant/fungal samples, a more realistic FEFF model (Rehr et al., 1992) was built to describe the EXAFS spectrum of the reference Hg-cysteine complex, which best resembled the plant spectra, but provided useful data in k-space out to 13 Å^{-1}. The Hg EXAFS model takes into account two possible Hg complexations with cystein molecules (Fig. 6a). The dominant way of complexation is attachment of two cysteine molecules on Hg cation *via* thiol groups (–SH) in diametric positions (Fig. 6b). The alternative way of complexation is bonding of Hg on amino groups (–NH$_2$) between two cysteine molecules (Fig. 6c). Hg was known to attach preferably to nitrogen in heterocyclic groups as in histidine or in nucleotide bases; complexation with NH$_3$ or NH$_4$ is, however, also reported in chemistry textbooks (Greenwood and Earnshaw, 1984).

The FEFF model included two S atoms at the opposite sides of Hg, and two C atoms farther out in accord with tentative distances in the Hg–S–C triangle. To test the possibility of Hg complexation to amino groups we introduced in FEFF *ansatz* two opposing –N–C ligand groups, again taking into account the tentative interatomic distances. The full model comprised two single-scattering (SS) paths and six multiple scattering (MS) paths from the thiol groups, and two SS paths and three MS paths from the amino group. The MS paths, among them a strong focusing –S–Hg–S– path, were retained to account for a distinct side peak at ~4 Å in the cysteine FT spectrum, and present also in the spectra of most plant samples (Fig. 4).

The model provided a perfect fit over the entire interval (Fig. 7). It confirmed the antipodal placement of the two S: focusing paths are strongly sensitive to this placement, their amplitude decreasing strongly with any deviation from the linear arrangement of the atoms. As a modelling routine, the path was equipped with a multiplicative parameter to detect such a decrease: in the fit of Hg-cysteine spectrum, the value of the parameter remained close to 1.

The relative weights of the two ligand groups show that 16% of Hg atoms in the cysteine complex is attached to nitrogen. It should be noted that the model implies independent ligands, not thiol and amino groups from the same cysteine molecule.

We also tested the possibility of Hg binding to oxygen in the cysteine carboxylic group –COOH, instead of N from the amino group –NH$_2$. The attempt with two opposing –O–C ligand groups,

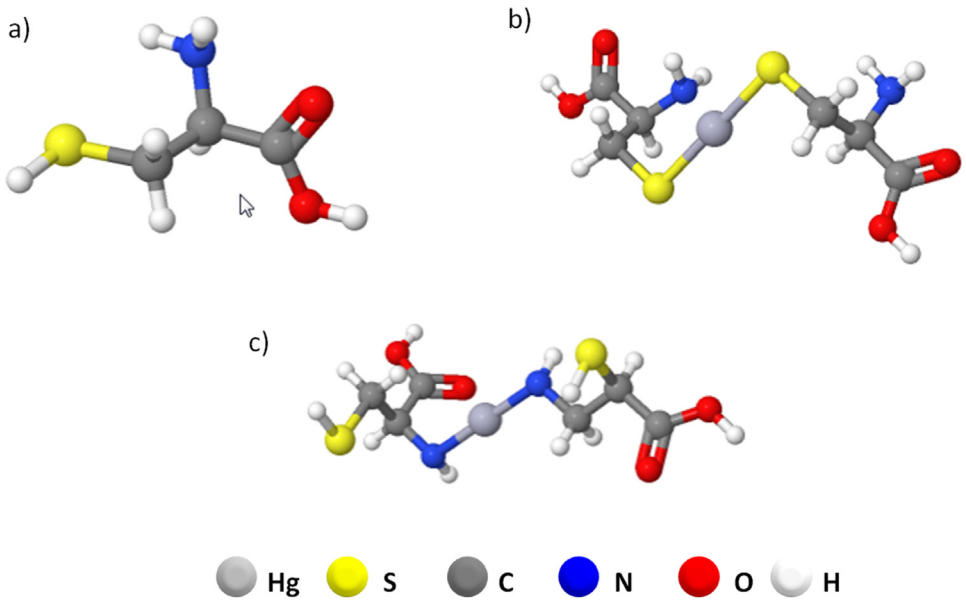

Fig. 6. Structural models of a) cysteine molecule, b) Hg coordination to two cysteine molecules *via* thiol (-SH) group, c) Hg coordination to two cysteine molecules *via* amino ($-NH_2$) group.

modelling the geometry of the atoms in the $-$COOH group, resulted in a much less satisfactory fit.

3.5. EXAFS on plant samples

The C-S-Hg-S-C/C-N-Hg-N-C model, developed on cysteine, was applied to the plant samples. It described satisfactorily the non-inoculated samples Con, ConI and ConC providing that the number of carbon atoms from the –N–C group was left to n available only in the amino group, the number was properly let fixed at one C per N atom. In the living plants, however, Hg complexation with nitrogen in heterocyclic amines, where N is attached to two C neighbours (as in histidine molecule), could contribute or even prevail the Hg–N–C signal from amino groups. Thus, merely letting the coordination number of C to vary freely not only adapted the model to either possibility but also provided a measure of their relative strength.

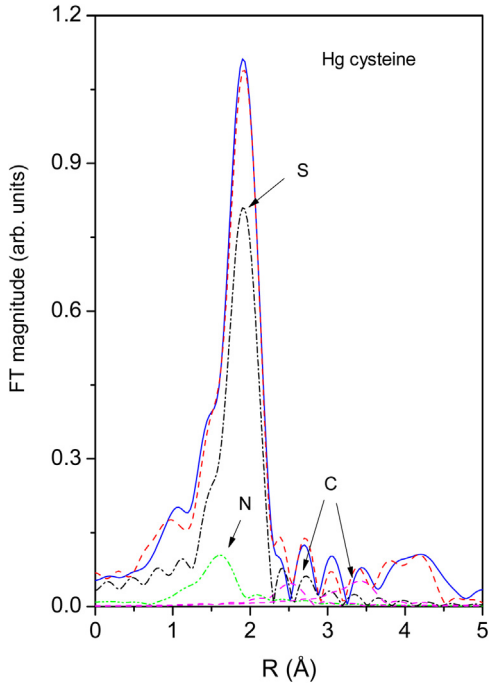

Fig. 7. Fourier transform magnitudes of the k^3 weighted Hg-L_3 edge EXAFS spectrum measured on Hg-cysteine (solid line), together with best-fit EXAFS model (dashed line), and the contributions of the individual neighbour shells: sulphur (black dash–dot line); nitrogen (green dash–dot–dot line); carbon (pink dashed line). (For interpretation of the references to colour in this figure legend, the reader is referred to the web version of this article.)

In the fungal sample (Fung) and, to a lesser extent, in the inoculated samples AmI and AmC, the trend to increased S distance in the fits was detected. Not to compromise the standard model of Hg complexation to two thiol (–S–C) ligands, we introduced in the EXAFS model another possible Hg complexation to 4 thiol groups in tetrahedral arrangement, where the Hg-S distance (∼2.50 Å) and Hg-C distance (∼4.3 Å) are larger than in case of Hg complexation to two thiol groups The tetra-cysteine ligand group has been reported recently by (Manceau and Nagy, 2008; Thomas and Gaillard, 2015) in a study of Hg in *E. Coli*. They found that Hg-tetra-cysteine complex is present only in metabolically active cells and is lost during lysis.

To improve the fit statistics all six plant spectra were fitted simultaneously with a single set of path parameters – in line with the hypothesis that identical Hg complexes were present in all the samples – so that the spectra were satisfactorily described just as linear combinations of the three Hg model neighbourhood environments: di-thiol ligands Hg–$(S–C)_2$, tetra-thiol ligands Hg –$(S–C)_4$, and two amino ligands Hg–$(N–C)_2$, varying their relative amplitudes.

The collective model with three Hg complexes is sufficiently flexible to reproduce the data from six plant/fungal samples in the entire interval from 1 to 4.4 Å. It comprises variable parameters for the relative frequencies of the three complexes in each spectrum, the common parameters ΔR and σ^2 for each ligand group, two parameters for the strength of the focusing paths –S–Hg–S– and –N–Hg–N–, and the standard EXAFS parameters of the shift of the photoelectron energy origin ΔE_0 and amplitude reduction factor S_0^2. The latter is fixed at the value 0.93, determined in the cysteine fit and in perfect agreement with the value from the seminal

analysis of Hg attachment to DNA (Ravel et al., 2009). The coordination numbers of S and C in the thiol groups are restricted to the same value. Similar restrictions are applied to some σ^2 parameters to stabilize the fit. The coordination numbers of N and C atoms in the Hg—N—C groups are varied separately to describe the two possible Hg complexations with nitrogen ligands in heterocyclic amines, or in amino groups.

As seen in the plots (Figs. 3 and 4) the fits describe well the measured spectra. The parameters of the immediate ligands S and N are recovered with high reliability, while the uncertainties are larger for carbon neighbour parameters in second coordination shells. The best fit model parameters are collected in Table 6.

In all plant samples, at least 73% of Hg is attached to thiol-groups. In non-mycorrhizal Con, ConC and ConI samples only complexation with two thiol groups at the short Hg-S distance is found. The tetra-thiol complexation of Hg with longer Hg-S distance prevails in the Fung sample (64%), is strong in AmI (26%), and moderate in AmC sample (21%). The short Hg-S distance in the di-thiolate complex stays within 0.015 Å of the value in cysteine (2.34 Å), while the Hg-S distance in the tetra-thiolate Hg complex is significantly longer (2.50 Å). The Hg-N distance is kept fixed at the histidine value. The ratio between the number of carbon atoms C_N bound to N is above one in ConC and ConI, which indicates complexation of Hg with heterocyclic amines, where N is attached to two carbon atoms (as in the histidine molecule). In mycorrhizal samples the C_N/N ratio is close to one, indicating the complexation of Hg to amino goups as in cysteine. The finding is correlated with the presence of tetra-thiol Hg complexes in the Fung, AmI, and AmC samples.

The EXAFS results are in agreement with XANES findings. The fungal endophyte sample (Fung), which has a prevailing amount of the tetra-thiol Hg complex, exhibits significantly different Hg L_3 XANES profile, not fully describable by a linear combination of reference XANES spectra of Hg-cysteine and Hg-histidine complexes. The relative amount of tetra-thiol Hg complexes in the plant samples can be estimated if Fung XANES spectrum is used as a reference in the LCF analysis (Table 5). As shown by EXAFS analysis the Fung sample contains 64% of tetra-thiol Hg complex, 13% of di-thiol complex (as in Hg-cystein) and 24% complex with amino ligands.

4. Discussion

4.1. Mycorrhization and Hg root uptake

In both AM inoculated plant groups (AmC and AmI) the fungi formed typical AM structures as arbuscules and vesicles. However in AmI the formation of arbuscules was more prominent than in AmC, while in the later more vesicles were observed, indicating that the AM fungi from the vicinity of Hg mine in Idrija are more tolerant to Hg that those from commercial inoculum.

AM fungi isolated at the Hg polluted site in Idrija significantly increased Hg root uptake which is not in line with Yu et al. (2010) who showed that mycorrhizal inoculation by AM fungi *Glomus mossae* increased immobilization of Hg in soil and reduced the uptake of Hg by roots, possibly *via* Hg bonding to extramatrical mycelium; and neither with a conceptual model proposed by Audet and Charest (2007) according to which AM fungi reduce metal bioavailability through metal-binding processes at high soil-metal levels (1–10^4 mg kg^{-1} dry soil), hence resulting in increased plant biomass and enhanced plant tolerance through heavy metal stress avoidance. It has to be emphasized that in the experiment by Yu et al. (2010) much lower Hg concentrations were used. In our study Hg concentrations typically measured in the vicinity of the cinnabar mine and smelter in Idrija (Kocman et al., 2004; Miklavčič et al., 2013) were applied, in order to mimic natural conditions and to provide sufficient amount of Hg in the samples for application of XAS techniques.

There was a decrease of root biomass in AmI plants. Since the production of hyphae is much more economical in terms of organic C than the production of an equivalent length of a root, plants may thus also adjust below-ground C allocation and manage with a smaller mycorrhizal root system (Jakobsen et al., 2003).

4.2. Hg ligand environment in plants and fungi

In plant samples the amount of tetra-thiol ligand correlates well with the level of arbuscular formation – the sites of nutrient exchange between plant and fungi – and increased Hg concentration in the roots (Fig. 8) indicating that mycorrhization may affect soil-to-root Hg mobility and Hg root uptake through modification of Hg ligand environment. Interactions of AM fungi with heavy metals are considerably well studied, but the results remain controversial. In some studies increased metal concentrations in plants tissues are found in presence of AM fungi, while some others claim the opposite (Audet and Charest, 2007). Only few studies, though, examined the speciation of metals in mycorrhizal and non-mycorrhizal plants (Rhee et al., 2012) from the perspective of the mechanisms of metal-soil-fungi-plant interactions.

Our findings are in accord with the established fact that the linear –C–S–Hg–S–C– coordination at the Hg-S distance of 2.35 Å is the strongest and the most stable among Hg complexes observed in the studied plant and fungal material (Lin et al., 2012). Tetra-thiol Hg complexation is predominant in fungal sample (Fung) and strong in plant roots inoculated with AM fungi from Idrija (AmI), correlating positively with Hg root concentrations. This indicates that fungi are able to take up and transport Hg from soil to the plant roots more efficiently than plants themselves, probably by transforming Hg to more mobile forms.

Formation of HgS in extramatrical fungal mycelium as originally hypothesized would on the other hand lower Hg mobility and consequentially decrease Hg concentration in the roots. A FEFF model based on the crystallographic data of a trigonal HgS (P 32 2 1 space group with unit cell parameters a = 4.1450 Å, b = 4.1450 Å, c = 9.4960 Å), containing 7 SS scattering paths to 3 S and 4 Hg neighbours, was constructed and successfully tested in a fit of EXAFS spectrum measured on cinnabar from the Idrija mine. With the same model alone, 4 out of 6 plant samples could be reproduced surprisingly well, with the quality-of-fit close to 1%. The fits produced different combinations of the model parameters, which precluded the general presence of HgS in the samples. However, the test showed how easy it would be to “prove” the mineral in the plant tissues. For this reason special attention needs to be paid when analysing Hg-L_3 XANES/EXAFS spectra of biological origin.

Since Hg EXAFS and XANES are only able to resolve the nature of the atoms in the first and second coordination shell, further studies are needed to resolve which sulphur compounds play a role in Hg chelation. In the presence of heavy metals plants as well as fungi are known to synthesize phytochelatins (Type III metallothioneins) as well as other metallothioneins (Henkel and Krebs, 2004; Nagy et al., 2011). A direct correlation between Hg plant concentrations and phytochelatins was confirmed in plants growing at the vicinity of Almaden Hg mine (Dago et al., 2014). In addition low molecular weight thiols such as glutathione and cystein may also play important role in Hg chelation (Carrasco-Gil et al., 2013; Meng et al., 2014). In plants Hg was reported to be mainly sequestered in the cell wall and bound to cell-wall S- containing proteins (Carrasco-Gil et al., 2013). Binding to cysteine or glutathione stored in the root cell wall as reported by Carrasco-Gill et al., would support di-thiolate (–C–S–Hg–S–C–) coordination seen in non-inoculated (ConC & ConI) plants in this experiment.

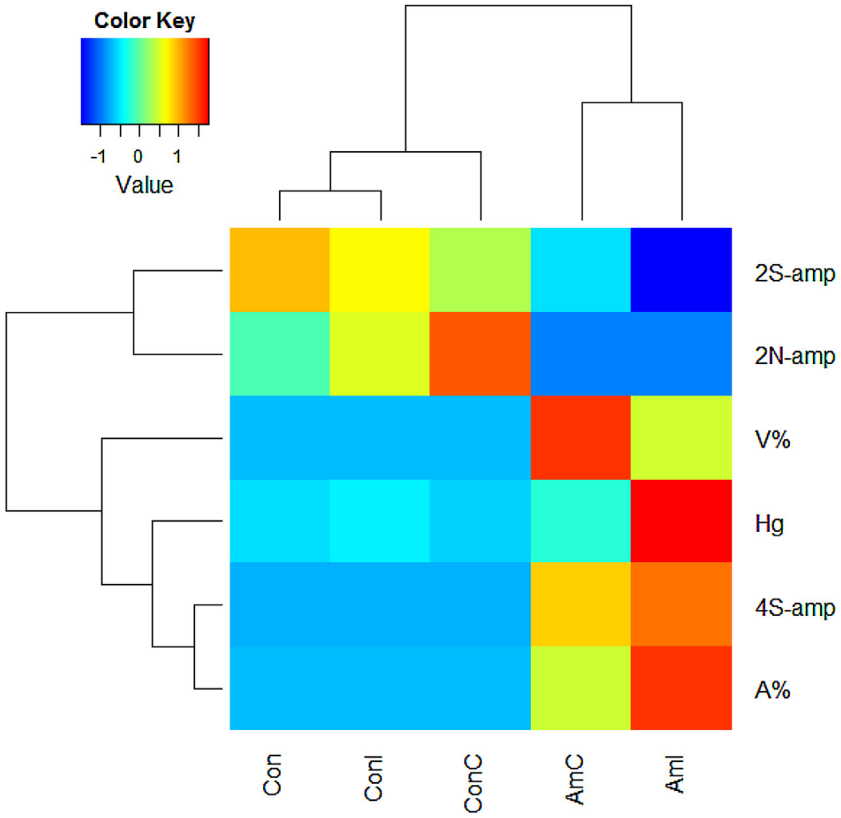

Fig. 8. Heat map with two way clustering (Euclidian distance) showing the relationships between AM parameters (A%- arbuscular density, V% – vesicular density), Hg concentrations and the amplitudes of di-thiolate (2S), tetra-thiolate (4S) and di-amino (2N) Hg ligands. Data were z-scaled prior to clustering- Colour scale: blue – low values, green and yellow – middle values, red –high values (For interpretation of the references to colour in this figure legend, the reader is referred to the web version of this article.)

Little information is available on metal detoxification mechanisms in mycorrhizal fungi. The occurrence of metallothioneins (MTs) and PCs, or both, is still a matter of debate. In a study by Lanfranco et al. a MT like polypeptide designated GmarMT1 was identified in AM fungus *Glomus margarita*, conferring tolerance to Cu and Cd, raising questions whether mycobiont-derived MTs can confer an increased tolerance to the host plants (Lanfranco et al., 2002). Similarly as in plants, in fungi the cell wall may provide Hg binding sites; however uptake across plasma membrane cannot be excluded, especially because of the enhanced Hg uptake to the roots of mycorrhizal (AmI, AmC) *vs.* the control (Con, ConC & ConI) plants. High proportion of tetra-thiolate complexes seen in fungal and AM samples would support Hg fungal cell internalization and binding to metallothioneins or phytochelatins, known to form metal-tetrathiolate complexes (Henkel and Krebs, 2004; Lanfranco et al., 2002). In addition glutathione has a high tendency to form tri- and tetra- thiolate complexes (Mah and Jalilehvand, 2008). At large excess of free glutathione ($[GS^{3-}] > 140\,mmol\,dm^{-3}$) at ambient temperature, 30% of the Hg(II) was present in the form of a tetra-thiolate complex $[Hg(GS)_4]$ (Mah and Jalilehvand, 2008) with a mean Hg–S distance of 2.52(2) Å. Recently a study on symbiosis between *Nicotiana tabacum* and AM fungi *Funneliformis* (*Glomus*) *mosseae* reported on increased levels of glutathione in mycorrhizal *vs.* non-mycorrhizal plants (Degola et al., 2015) further supporting our observation.

5. Conclusions

In non-mycorrhizal roots Hg is mainly bound in di-thiolate and di-amino complexes, while in AM roots Hg tetra-thiolate complexes are also seen. The percentage of Hg tetra- thiolate complexes formed correlates intensively with the level of arbuscular formation and Hg root concentrations, indicating that AM fungi can alter Hg ligand environment and Hg soil to root mobility. Further studies are needed, however, to more precisely identify the molecular nature of sulphur Hg ligands in plants and AM fungi.

According to our results Hg tolerant AM strains could be suitable for phytostabilization of Hg contaminated soils, since the enhanced soil to root Hg mobility and Hg root accumulation capacity may decrease Hg leaching and volatilization.

Acknowledgements

Study was financed by the Slovenian Research Agency programmes (P1-0212, P1-0112 and P3-0395) and the IAEA framework of coordinated research projects RC 16796 “Applications of synchrotron radiation for environmental sciences and materials research for development of environmentally friendly resources” (CSI, Katarina Vogel-Mikuš). The European Synchrotron Radiation Facility (ESRF), Grenoble, France, is acknowledged for provision of synchrotron radiation facilities at beamline BM23 (projects LS-2209 and LS- 2275) and of ELETTRA for provision of synchrotron radiation facilities at beamline XAFS, (project 20115112). The authors are grateful to ESRF staff Gleb Parakhonskiy, Antonella Iadecola and Olivier Mathon for assistance in using beamline BM23, and Giuliana Aquilanti and Luca Olivi of ELETTRA, for support and expert advice on XAFS beamline operation. Dr. Bojan Budič from National Chemical Institute is acknowledged for the help with ICP-MS measurements.

References

Adriano, D.C., 2001. Trace Elements in Terrestrial Environments: Biogeochemistry, Bioavailability, and Risks of Metals. Springer-Verlag, New York, N.Y.

Altschul, S.F., Madden, T.L., Schäffer, A.A., Zhang, J., Zhang, Z., Miller, W., Lipman, D.J., 1997. Gapped BLAST and PSI-BLAST: a new generation of protein database search programs. Nucleic Acids Res. 25, 3389–3402.

Arai, T., Ikemoto, T., Hokura, A., Terada, Y., Kunito, T., Tanabe, S., Nakai, I., 2004. Chemical forms of mercury and cadmium accumulated in marine mammals and seabirds as determined by XAFS analysis. Environ. Sci. Technol. 38, 6468–6474.

Audet, P., Charest, C., 2007. Dynamics of arbuscular mycorrhizal symbiosis in heavy metal phytoremediation: meta-analytical and conceptual perspectives. Environ. Pollut. 147, 609–614.

Barceló, J., Poschenrieder, C., 2003. Phytoremediation: principles and perspectives. Contributions to Science, 2. Institut d'Estudis Catalans, Barcelona, pp. 333–344.

Calvente, R., Cano, C., Ferrol, N., Azcón-Aguilar, C., Barea, J., 2004. Analysing natural diversity of arbuscular mycorrhizal fungi in olive tree *(Olea europaea* L:) plantations and assessment of the effectiveness of native fungal isolates as inoculants for commercial cultivars of olive plantlets. Appl. Soil Ecol. 26, 11–19.

Carrasco-Gil, S., Siebner, H., Leduc, D.L., Webb, S.M., Millán, R., Andrews, J.C., Hernández, L.E., 2013. Mercury localization and speciation in plants grown hydroponically or in a natural environment. Environ. Sci. Technol. 47, 3082–3090.

Clarkson, T.W., 1972. The biological properties and distribution of mercury. Biochem. J. 130, 61–63.

Dago, À., González, I., Ariño, C., Martínez-Coronado, A., Higueras, P., Díaz-Cruz, J.M., Esteban, M., 2014. Evaluation of mercury stress in plants from the Almadén mining district by analysis of phytochelatins and their Hg complexes. Environ. Sci. Technol. 48, 6256–6263.

Debeljak, M., van Elteren, J.T., Vogel-Mikuš, K., 2013. Development of a 2D laser ablation inductively coupled plasma mass spectrometry mapping procedure for mercury in maize (*Zea mays* L.) root cross-sections. Anal. Chim. Acta 787, 155–162.

Degola, F., Fattorini, L., Bona, E., Sprimuto, C.T., Argese, E., Berta, G., Sanità di Toppi, L., 2015. The symbiosis between *Nicotiana tabacum* and the endomycorrhizal fungus Funneliformis mosseae increases the plant glutathione level and decreases leaf cadmium and root arsenic contents. Plant Physiol. Biochem. 92, 11–18.

Gaur, A., Varma, A., 2007. Research methods in arbuscular mycorrhizal fungi. Advanced Techniques in Soil Microbiology. Springer, Berlin Heidelberg, Berlin, Heidelberg, pp. 377–396.

Gräfe, M., Donner, E., Collins, R.N., Lombi, E., 2014. Speciation of metal(loid)s in environmental samples by X-ray absorption spectroscopy: a critical review. Anal. Chim. Acta 822, 1–22.

Greenwood, N.N., Earnshaw, A., 1984. Chemistry of the Elements. Butterworth-Heinemann.

Helgason, T., Daniell, T.J., Husband, R., Fitter, A.H., Young, J.P.W., 1998. Ploughing up the wood-wide web? Nature 394, 431-431.

Henkel, G., Krebs, B., 2004. Metallothioneins: zinc, cadmium, mercury, and copper thiolates and selenolates mimicking protein active site features – structural aspects and biological implications. Chem. Rev. 104, 801–824.

Jakobsen, I., Smith, S.E., Smith, F.A., 2003. Function and Diversity of Arbuscular Mycorrhizae in Carbon and Mineral Nutrition. Springer, Berlin Heidelberg, pp. 75–92.

Kimura, M., 1980. A simple method for estimating evolutionary rates of base substitutions through comparative studies of nucleotide sequences. J. Mol. Evol. 16, 111–120.

Kocman, D., Horvat, M., Kotnik, J., 2004. Mercury fractionation in contaminated soils from the Idrija mercury mine region. J. Environ. Monit. 6, 696–703.

Kodre, A., Vogel-Mikuš, K., Arčon, I., Debeljak, M., 2015. EXAFS study of mercury ligand environment in mycorrhizal plant roots. The 16th International Conference on X-Ray Absorption Fine Structure, 23–28 August, 2015, Karlsruhe: Program, pp. 92.

Koren, Š., Arčon, I., Kump, P., Nečemer, M., Vogel-Mikuš, K., 2013. Influence of $CdCl_2$ and $CdSO_4$ supplementation on Cd distribution and ligand environment in leaves of the Cd hyperaccumulator *Noccaea (Thlaspi) praecox*. Plant Soil 370, 125–148.

Kumar, S., Stecher, G., Tamura, K., 2016. MEGA7: molecular Evolutionary Genetics Analysis Version 7.0 for Bigger Datasets. Mol. Biol. Evol. 33, 1870–1874.

Lanfranco, L., Bolchi, A., Ros, E.C., Ottonello, S., Bonfante, P., 2002. Differential expression of a metallothionein gene during the presymbiotic versus the symbiotic phase of an arbuscular mycorrhizal fungus. Plant Physiol. 130, 58–67.

Likar, M., Regvar, M., 2013. Isolates of dark septate endophytes reduce metal uptake and improve physiology of *Salix caprea* L. Plant Soil 370, 593–604.

Lin, X., Brooks, J., Bronson, M., Ngu-Schwemlein, M., 2012. Evaluation of the association of mercury(II) with some dicysteinyl tripeptides. Bioorg. Chem. 44, 8–18.

Mah, V., Jalilehvand, F., 2008. Mercury(II) complex formation with glutathione in alkaline aqueous solution. J. Biol. Inorg. Chem. 13, 541–553.

Manceau, A., Nagy, K.L., 2008. Relationships between Hg(II)-S bond distance and Hg (II) coordination in thiolates. Dalton Trans 1421–1425.

Meng, B., Feng, X., Qiu, G., Anderson, C.W.N., Wang, J., Zhao, L., 2014. Localization and speciation of mercury in brown rice with implications for pan-Asian public health. Environ. Sci. Technol. 48, 7974–7981.

Miklavčič, A., Mazej, D., Jaćimović, R., Dizdarevič, T., Horvat, M., 2013. Mercury in food items from the Idrija Mercury Mine area. Environ. Res. 125, 61–68.

Morel, F.M.M., Kraepiel, A.M.L., Amyot, M., 1998. The chemical cycle and bioaccumulation of mercury. Annu. Rev. Ecol. Syst..

Nagy, K.L., Manceau, A., Gasper, J.D., Ryan, J.N., Aiken, G.R., 2011. Metallothionein-like multinuclear clusters of mercury(II) and sulfur in peat. Environ. Sci. Technol. 45, 7298–7306.

Nečemer, M., Kump, P., Ščančar, J., Jaćimović, R., Simčič, J., Pelicon, P., Budnar, M., Jeran, Z., Pongrac, P., Regvar, M., Vogel-Mikuš, K., 2008. Application of X-ray fluorescence analytical techniques in phytoremediation and plant biology studies. Spectrochim. Acta B Atomic Spectrosc. 63, 1240–1247.

Patty, C., Barnett, B., Mooney, B., Kahn, A., Levy, S., Liu, Y., Pianetta, P., Andrews, J.C., 2009. Using x-ray microscopy and Hg L3 XANES to study Hg binding in the rhizosphere of spartina cordgrass. Environ. Sci. Technol. 43, 7397–7402.

Phillips, J.M., Hayman, D.S., 1970. Improved procedures for clearing roots and staining parasitic and vesicular-arbuscular mycorrhizal fungi for rapid assessment of infection. Trans. Br. Mycol. Soc. 55, 158-IN18.

Rajan, M., Darrow, J., Hua, M., Barnett, B., Mendoza, M., Greenfield, B.K., Andrews, J. C., 2008. Hg L 3 XANES Study of Mercury Methylation in Shredded *Eichhornia crassipes*. Environ. Sci. Technol. 42, 5568–5573.

Rajkumar, M., Sandhya, S., Prasad, M.N.V., Freitas, H., 2012. Perspectives of plant-associated microbes in heavy metal phytoremediation. Biotechnol. Adv. 30, 1562–1574.

Ravel, B., Newville, M., 2005. ATHENA, ARTEMIS, HEPHAESTUS: data analysis for X-ray absorption spectroscopy using IFEFFIT. J. Synchrotron Radiat. 12, 537–541.

Ravel, B., Slimmer, S.C., Meng, X., Wong, G.C.L., Lu, Y., 2009. EXAFS studies of catalytic DNA sensors for mercury contamination of water. Radiat. Phys. Chem. 78, 75–79.

Rehr, J.J., Albers, R.C., Zabinsky, S.I., 1992. High-order multiple-scattering calculations of x-ray-absorption fine structure. Phys. Rev. Lett. 69, 3397–3400.

Rhee, Y.J., Hillier, S., Gadd, G.M., 2012. Lead transformation to pyromorphite by fungi. Curr. Biol. 22, 237–241.

Santos-González, J.C., Finlay, R.D., Tehler, A., 2007. Seasonal dynamics of arbuscular mycorrhizal fungal communities in roots in a seminatural grassland. Appl. Environ. Microbiol. 73, 5613–5623.

Simon, L., Lalonde, M., Bruns, T.D., 1992. Specific amplification of 18S fungal ribosomal genes from vesicular-arbuscular endomycorrhizal fungi colonizing roots. Appl. Environ. Microbiol. 58, 291–295.

Singh, S.P., Vogel-Mikuš, K., Vavpetič, P., Jeromel, L., Pelicon, P., Kumar, J., Tuli, R., 2014. Spatial X-ray fluorescence micro-imaging of minerals in grain tissues of wheat and related genotypes. Planta 240, 277–289.

Thomas, S.A., Gaillard, J.-F., 2015. Effect of Organic ligands and cell metabolism on Hg(II) sorption and coordination to E. coli. Goldschmidt Abstracts, , pp. 3116.

Trouvelot, A., Kough, J.L., Gianinazzi-Pearson, V., 1986. Estimation of VA mycorrhizal infection levels. Research for methods having a functional significance. Physiological and Genetical Aspects of Mycorrhizae. Aspects physiologiques et genetiques des mycorhizes, Dijon (France), 1–5 Jul 1985./1INRA.

Vandenkoornhuyse, P., Leyval, C., 1998. SSU rDNA Sequencing and pcr-fingerprinting reveal genetic variation within *Glomus mosseae*. Mycologia 90, 791.

Vogel-Mikuš, K., Arčon, I., Kodre, A., 2010. Complexation of cadmium in seeds and vegetative tissues of the cadmium hyperaccumulator *Thlaspi praecox* as studied by X-ray absorption spectroscopy. Plant Soil 331, 439–451.

Wong, J., Lytle, F.W., Messmer, R.P., Maylotte, D.H., 1984. K –edge absorption spectra of selected vanadium compounds. Phys. Rev. B 30, 5596–5610.

Yu, Y., Zhang, S., Huang, H., 2010. Behavior of mercury in a soil–plant system as affected by inoculation with the arbuscular mycorrhizal fungus Glomus mosseae. Mycorrhiza 20, 407–414.